

Theory of Nonlinear Magneto-Optics

U. Pustogowa, T. A. Luce, **W. Hübner**, and K. H. Bennemann

*Institute for Theoretical Physics, Freie Universität Berlin, Arnimallee 14, D - 14195 Berlin,
Germany*

Abstract

Nonlinear magneto-optics is a very sensitive fingerprint of the electronic, magnetic, and atomic structure of surfaces, interfaces, and thin ferromagnetic films. Analyzing theoretically the nonlinear magneto-optical Kerr effect for thin films of Fe(001) and at Fe surfaces we demonstrate exemplarily how various electronic material properties of ferromagnets, such as the d -band width, the magnetization, the substrate lattice constant, and the film-thickness dependence can be extracted from the calculated nonlinear Kerr spectra. Furthermore, we show how the substrate d electrons (Cu(001)) affect the nonlinear Kerr spectra even without being themselves spin-polarized and without film-substrate hybridization. We show that the Kerr rotation angle in second harmonic generation is enhanced by one to two orders of magnitude compared to the linear Kerr angle and how symmetry can be used to obtain the direction of magnetization in thin films and at buried interfaces from nonlinear magneto-optics.

75.30.Pd,78.20.Ls,73.20.At,75.50.Bb

I. INTRODUCTION

Nonlinear magneto-optics for metals [1,2] is a new expanding field the significance of which results from extending electrodynamics to the nonlinear case and from applications. Particularly, an important task of theory was to extend the symmetry analysis to an electronic theory [3,4] since this allowed second harmonic generation (SHG) to be used as an important new tool for the analysis of surface [5], interface, thin film, and multilayer [6,7] magnetism. The surface sensitivity results since breakdown of inversion symmetry is necessary for SHG. Thus, it is possible to determine with the help of SHG surface magnetic moments, magnetic anisotropy, domains, magnetostriction, and, in particular, properties of buried interfaces.

Using an electronic theory (with a bandstructure input) we calculate (i) the material specific nonlinear response function $\chi^{(2)}(\omega, \mathbf{M}, \lambda_{s.o.}, d)$, depending on magnetization M , spin-orbit coupling $\lambda_{s.o.}$ and film thickness d , (ii) the nonlinear Fresnel formula for the reflected nonlinear fields $E(2\omega)$, and thus finally, (iii) the complex nonlinear Kerr rotation angle $\Phi_K^{(2)}$. The results, presented in the following demonstrate, in particular, what can be learned (a) from an analysis of the frequency dependence and (b) from the symmetry analysis and the Kerr rotation. Some selected general results obtained previously are shown, but also interesting new results indicating important substrate effects. Remarkably, the calculation [8] and recent experiments [9,10] yield that $\Phi_K^{(2)}$ is larger by two orders of magnitude compared to the linear Kerr rotation.

II. THEORY

A. Nonlinear susceptibility

Using response theory the nonlinear optical polarization is given by

$$P_i = \chi_{ijm}^{(2)} E_j(\omega) E_l(\omega), \quad (1)$$

where P_i is the i -th component of the polarizability and where the susceptibility tensor $\chi_{ijl}^{(2)}$ is determined by [1,11]

$$\begin{aligned}
\chi_{ijm}^{(2)}(2q_{\parallel}, 2\omega, \mathbf{M}) &= \frac{e^3 C \lambda_{s.o.}}{\Omega \hbar \omega} \\
&\times \sum_{\sigma} \sum_{\mathbf{k}, l, l''} \left\{ \langle \mathbf{k} + 2\mathbf{q}_{\parallel}, l'' \sigma | i | \mathbf{k} l \sigma \rangle \langle \mathbf{k} l \sigma | j | \mathbf{k} + \mathbf{q}_{\parallel}, l' \sigma \rangle \langle \mathbf{k} + \mathbf{q}_{\parallel}, l' \sigma | m | \mathbf{k} + 2\mathbf{q}_{\parallel}, l'' \sigma \rangle \right. \\
&\times \left. \frac{\frac{f(E_{\mathbf{k}+2\mathbf{q}_{\parallel}, l'' \sigma}) - f(E_{\mathbf{k}+\mathbf{q}_{\parallel}, l' \sigma})}{E_{\mathbf{k}+2\mathbf{q}_{\parallel}, l'' \sigma} - E_{\mathbf{k}+\mathbf{q}_{\parallel}, l' \sigma} - \hbar\omega + i\hbar\alpha_1} - \frac{f(E_{\mathbf{k}+\mathbf{q}_{\parallel}, l' \sigma}) - f(E_{\mathbf{k}l \sigma})}{E_{\mathbf{k}+\mathbf{q}_{\parallel}, l' \sigma} - E_{\mathbf{k}l \sigma} - \hbar\omega + i\hbar\alpha_1}}{E_{\mathbf{k}+2\mathbf{q}_{\parallel}, l'' \sigma} - E_{\mathbf{k}l \sigma} - 2\hbar\omega + i2\hbar\alpha_1}} \right\}. \quad (2)
\end{aligned}$$

Here $E_{\mathbf{k}l\sigma}$ are the electronic energy levels resulting from the bandstructure calculations, $\langle \mathbf{k}l\sigma | i | \mathbf{k} + \mathbf{q}_{\parallel}, l' \sigma \rangle$ are the transition matrix elements, which control the symmetry and thus the interface sensitivity. If the matrix elements are treated as constants one has to introduce a cut-off to guarantee the surface sensitivity. This is done by the factor C [12]. Typically, magnetic dipole effects are negligible if the electric dipole contribution does not vanish. $\lambda_{s.o.}$ is the key parameter for nonlinear magneto-optics. In particular, for determining the Kerr effect it might be useful to decompose $\chi^{(2)}$ in odd and even contributions $\chi^{(2)} = \chi^{(2)}(\mathbf{M}) + \chi^{(2)}(M^2)$.

For the application of the general theory thin films are of particular interest. Then, the layer-dependent contributions to $\chi^{(2)}$ reveal interesting film properties and substrate effects. For the thin film calculations we use $C = W_{\mathbf{k}+2\mathbf{q}_{\parallel}, l'' \sigma} W_{\mathbf{k}+\mathbf{q}_{\parallel}, l' \sigma} W_{\mathbf{k}l \sigma}$, where W_{α} denotes the weight of the density of state $|\mathbf{k}l\sigma\rangle$ in the Wigner-Seitz cell of the first monolayer. Note, due to the factor C SHG will always result from the surface layer or from the layer at the interface, however the electronic structure of this layer depends on the film thickness. The bandstructure $E_{\mathbf{k}l\sigma}$ is calculated employing the full-potential linear muffin-tin orbital method (FP-LMTO) [13] for thin Fe(001) films within a symmetric slab calculation.

Results for one, three, five, and seven layers of Fe are presented in Fig. 1. The depth of the first minimum in the spectra scales linearly with the magnetic moment of the top layer while the energy of this minimum reflects the d -band width. As can be seen from Fig. 2, the nonlinear spectra reveal the structural changes induced by different substrates or temperatures. In Fig. 3 we compare the *ab initio* nonlinear Kerr spectrum for the Fe(001) monolayer with tight-binding calculations. From the results of Fig. 3 it becomes obvious that it is necessary to use *ab initio* calculations for the films if only bulk tight-binding parameters are available. However, tight-binding calculations may be adequate if one uses as input parameters those determined from *ab initio* calculations for thin films.

We expect generally also interesting results for $\chi^{(2)}$ at heterogeneous interfaces like Fe/Cu(001). For example, it is of interest to find out how the substrate interferes with the electronic structure of the thin film. For this reason we performed calculations of the Fe/Cu bilayer. Results are shown in Fig. 4. The additional peak structure reveals the electronic influence even of the nonmagnetic Cu on the nonlinear magneto-optic response of thin films. This might be of general significance also with respect to the analysis of quantum well states (tuning of interface properties, $\lambda_{s.o.}$ in substrate, M in films).

From the results of Figs. 1 through 4 we learn that the nonlinear Kerr effect is a sensitive probe of the magnetic and electronic structure at interfaces.

B. Symmetry and Kerr rotation

That SHG is very symmetry sensitive is furthermore particular demonstrated by its polarization dependence and by the remarkable enhancement of the Kerr rotation [8]. The latter important result was first theoretically derived by Pustogowa *et al.* [8] and later observed in experiments by Böhmer *et al.* [9] and Koopmans *et al.* [10].

First, we note that due to the symmetry sensitivity already SHG exhibits a corresponding polarization dependence, which interestingly is very different for transition and noble metals [3]. The latter results, since *s* and *d* electrons feel the breakdown of inversion symmetry at the interface differently. This symmetry dependence mainly results from the matrix elements in $\chi^{(2)}$, see Eq. (2). The different possible optical excitations contributing to $\chi^{(2)}$ for noble and transition metals are illustrated in Fig. 5. Obviously, SHG yields interesting information on the electronic structure even for $M=0$ and when no Kerr effect is present. This area needs further analysis and might offer interesting new results [3].

Extending the symmetry analysis to the magnetic case we determine the Kerr rotations for different configurations and polarizations. The general analysis can be performed by using for *s* and *p* polarization (see [4])

$$E^{(2\omega)}(\Phi, \varphi) = 2i \left(\frac{\omega}{c} \right) |E_0^{(\omega)}|^2 \times \begin{pmatrix} A_p F_c \cos \Phi \\ A_s \sin \Phi \\ A_p N^2 F_s \cos \Phi \end{pmatrix} \chi_{ilm}^{(2)} \begin{pmatrix} f_c^2 t_p^2 \cos^2 \varphi \\ t_s^2 \sin^2 \varphi \\ f_s^2 t_p^2 \cos^2 \varphi \\ 2f_s t_p t_s \cos \varphi \sin \varphi \\ 2f_c f_s t_p^2 \cos^2 \varphi \\ 2f_c t_p t_s \cos \varphi \sin \varphi \end{pmatrix}, \quad (3)$$

where in the longitudinal configuration the susceptibility tensor is given by

$$\chi_{ilm}^{(2)} = \begin{pmatrix} 0 & 0 & 0 & | & 0 & \chi_{xzx}^{(2)} & \chi_{xyx}^{(2)} \\ \chi_{yxx}^{(2)} & \chi_{yyx}^{(2)} & \chi_{yzz}^{(2)} & | & \chi_{yyz}^{(2)} & 0 & 0 \\ \chi_{zxx}^{(2)} & \chi_{zyy}^{(2)} & \chi_{zzz}^{(2)} & | & \chi_{zyz}^{(2)} & 0 & 0 \end{pmatrix}, \quad (4)$$

and in the polar configuration by

$$\chi_{ilm}^{(2)} = \begin{pmatrix} 0 & 0 & 0 & | & \chi_{xyz}^{(2)} & \chi_{xzx}^{(2)} & 0 \\ 0 & 0 & 0 & | & \chi_{xzx}^{(2)} & -\chi_{xyz}^{(2)} & 0 \\ \chi_{zxx}^{(2)} & \chi_{zxx}^{(2)} & \chi_{zzz}^{(2)} & | & 0 & 0 & 0 \end{pmatrix}. \quad (5)$$

Here, Φ and φ denote the angles of polarization of the reflected frequency doubled and of the incident light, $A_{p,s}$ are the amplitudes, $f_{c,s}$ and $F_{c,s}$ are the Fresnel coefficients, and $t_{s,p}$ are the linear transmission coefficients for the fundamental light. Then, from

$$\phi_K^{(2)} \approx \text{Re} \frac{E_\varphi^{(2\omega)}(s - SH)}{E_\varphi^{(2\omega)}(p - SH)} \quad (6)$$

we determine the Kerr rotation for the polar and longitudinal configuration and for s and p polarized incident light. The following results are obtained:

For the longitudinal configuration (M_{\parallel}) and p (s) polarized incident light one gets

$$\phi_{K,p}^{(2)M_{\parallel}} = \text{Re} \frac{E_p^{(2\omega)}(s - SH)}{E_p^{(2\omega)}(p - SH)} = \text{Re} \frac{a_1 \chi_{yxx}^{(2)} + a_2 \chi_{yzz}^{(2)}}{a_3 \chi_{xzx}^{(2)} + a_4 \chi_{zxx}^{(2)} + a_5 \chi_{zzz}^{(2)}}, \quad (7)$$

$$\phi_{K,s}^{(2)M_{\parallel}} = \text{Re} \frac{E_s^{(2\omega)}(s - SH)}{E_s^{(2\omega)}(p - SH)} = \text{Re} \frac{a_6 \chi_{yyy}^{(2)}}{a_7 \chi_{zyy}^{(2)}}. \quad (8)$$

For the polar configuration (M_{\perp}) and p (s) polarized incident light one gets

$$\phi_{K,p}^{(2)M_{\perp}} = \text{Re} \frac{E_p^{(2\omega)}(s - SH)}{E_p^{(2\omega)}(p - SH)} = \text{Re} \frac{a_8 \chi_{xyz}^{(2)}}{a_9 \chi_{xxz}^{(2)} + a_{10} \chi_{zxx}^{(2)} + a_{11} \chi_{zzz}^{(2)}}, \quad (9)$$

$$\phi_{K,s}^{(2)M_{\perp}} = \operatorname{Re} \frac{E_s^{(2\omega)}(s - SH)}{E_s^{(2\omega)}(p - SH)} = \operatorname{Re} \frac{0}{a_{12}\chi_{zxx}^{(2)}}. \quad (10)$$

The coefficients $a_1 \dots a_{12}$ contain explicitly the whole information about the Kerr geometry (directions of light incidence and polarization, crystal magnetization) and about the linear transmission and reflection (see [4]).

Summarizing the results, we find that generally $\phi_K^{(2)M_{\perp}} > \phi_K^{(2)M_{\parallel}}$ and $\phi_{K,s}^{(2)} > \phi_{K,p}^{(2)}$, which is in agreement with the experiment by Koopmans *et al.* [10]. Numerical results of our theory using as input parameters the phase ratio of the various different tensor elements from Ni and linear complex indices of refraction are presented in Fig. 6. These results demonstrate clearly that the nonlinear Kerr angle depends sensitively on the direction of the magnetization and the incident beam, as well as on the light polarization. Depending on the experimental conditions the nonlinear Kerr angle might become even as large as 90° . Moreover, also the ellipticity will yield correspondingly large magnetic effects. From these results we conclude that the enhanced nonlinear Kerr rotation allows for the determination of easy axis and canted-spin configurations due to large magnetic contrast of different interfaces.

This selective discussion demonstrates the usefulness of nonlinear magneto-optics as a promising spectroscopy. Our results show that SHG is a new sensitive tool for determining magnetic interface properties such as the interplay of structure and magnetism, magnetic anisotropy, and magnetic reorientation. In contrast to linear optics, which probes characteristic film-averaged features, the nonlinear Kerr effect originates essentially from the surface and interfaces and thus allows the analysis of buried interfaces.

For future studies on the nonlinear magneto-optical Kerr effect it will be interesting to analyze magnetic anisotropy and easy axis, magnetic structure and domains, multilayers, and magnetostriction effects. Nonlinear optics at interfaces is a bulk-background-free technique and therefore, should yield a pronounced visibility of quantum well states and enhanced nonlinear paramagnetic Kerr oscillations in the presence of an external field.

An important future development of the nonlinear Kerr effect might result from femto-second dynamics which is able to follow the charge and spin dynamics of metallic interfaces in real time without involving the lattice.

REFERENCES

- ¹ W. Hübner and K. H. Bennemann, Phys. Rev. B **40**, 5973 (1989).
- ² R.P. Pan, H. D. Wei, and Y. R. Shen, Phys. Rev. B **39**, 1229 (1989).
- ³ W. Hübner, K. H. Bennemann, and K. Böhmer, Phys. Rev. B **50**, 17597 (1994).
- ⁴ W. Hübner and K. H. Bennemann, accepted for publication in Phys. Rev. B.
- ⁵ J. Reif, J. C. Zink, C. M. Schneider, and J. Kirschner, Phys. Rev. Lett. **67**, 2878 (1991).
- ⁶ H. A. Wierenga, M. W. J. Prins, D. L. Abraham, and Th. Rasing, Phys. Rev. B **50**, 1282 (1994).
- ⁷ H. A. Wierenga, W. de Jong, M. W. J. Prins, Th. Rasing, R. Vollmer, A. Kirilyuk, H. Schwabe, and J. Kirschner, Phys. Rev. Lett. **74**, 1462 (1995).
- ⁸ U. Pustogowa, W. Hübner, and K. H. Bennemann, Phys. Rev. B **49**, 10031 (1994); Appl. Phys. A **59**, 611 (1994).
- ⁹ K. Böhmer, J. Hohlfeld, and E. Matthias, Appl. Phys. A **60**, 203 (1995).
- ¹⁰ B. Koopmans, M. Groot Koerkamp, Th. Rasing, and H. van den Berg, Phys. Rev. Lett. **74**, 3692 (1995).
- ¹¹ W. Hübner, Phys. Rev. B **42**, 11553 (1990).
- ¹² U. Pustogowa, W. Hübner, K. H. Bennemann, submitted for publication.
- ¹³ M. Methfessel, Phys. Rev. B **38**, 1537 (1988); M. Methfessel, C. O. Rodriguez, and O. K. Andersen, *ibid.* **40**, 2009 (1989); M. Methfessel and M. Scheffler, Physica B **172**, 175 (1991).

FIGURES

FIG. 1. *Ab initio* calculated nonlinear magneto-optical Kerr spectra of Fe using Eq. (2) for a monolayer (dashed curve - 1), and films with 3 layers (dashed-dotted curve - 2), 5 layers (long-dashed - 3), and 7 atomic layers (dotted curve - 4). The second harmonic response results from the first atomic layer. This SH response is obtained by projecting the wave functions to the first atomic layer yielding the factor C .

FIG. 2. Film-lattice-constant dependence of *ab initio* calculated nonlinear Kerr spectra of a Fe monolayer. The solid curve refers to the bulk *bcc* Fe lattice constant $a=2.76 \text{ \AA}$, the dashed curve to $a=2.776 \text{ \AA}$ (bulk Au), and the dotted curve to $a=2.783 \text{ \AA}$ (bulk Ag). The long-dashed curve refers to the experimental $a=2.88 \text{ \AA}$ for Fe. Choosing lattice constants a referring to Au and Ag should simulate substrate effects. The inset shows for an enhanced scale the effects of different lattice constants for the zero of $\text{Im } \chi^{(2)}$ at $\hbar\omega \approx 3 \text{ eV}$ and indicate structural effects which should be observable.

FIG. 3. Comparison of *ab initio* (solid line - 2) and semi-empirical calculations of the nonlinear magneto-optical susceptibilities for a Fe monolayer. Semi-empirical calculations are performed for a two-dimensional atomic configuration (dashed-dotted curve - 1) and for a three-dimensional one with reduced hopping parameters (dashed curve - 3) containing the reduced coordination number of a monolayer compared to the bulk.

FIG. 4. Nonlinear magneto-optical Kerr-spectrum of a Fe/Cu bilayer system without (solid curve) and with (dashed curve) hybridization between the Fe and Cu layers. Note, the spectrum look rather different from the corresponding one for freestanding monolayers indicating a strong effect of Cu on the optical transitions.

FIG. 5. Illustration of second harmonic generation from noble metals [(a) and (b)] and transition metals [(c) and (d)]. For noble metals, in case (a) no d electrons can be optically excited, which in contrast is possible in case (b). In case (c) for transition metals, predominantly d electrons contribute to the SHG yield, whereas in case (d) the excitation starts from the s band. Note, the cases (a) and (c) refer to low-frequency excitations while (b) and (d) correspond to high-frequency excitation.

FIG. 6. Nonlinear Kerr rotation angles for p polarized incident light $\phi_{K,p}^{(2)}$ (full and short-dashed curves) and for s polarized incident light $\phi_{K,s}^{(2)}$ (long-dashed and dotted curves) for Fe at 770 nm as a function of the angle of incidence θ in the longitudinal Kerr configuration. The relative phase between $\chi_{zxx}^{(2)} = \chi_{zyy}^{(2)}$ and $\chi_{zzz}^{(2)}$ is $\varphi_1=0.505\pi$ in the full and long-dashed curves and $\varphi_2=1.505\pi$ in the short-dashed and dotted curves.

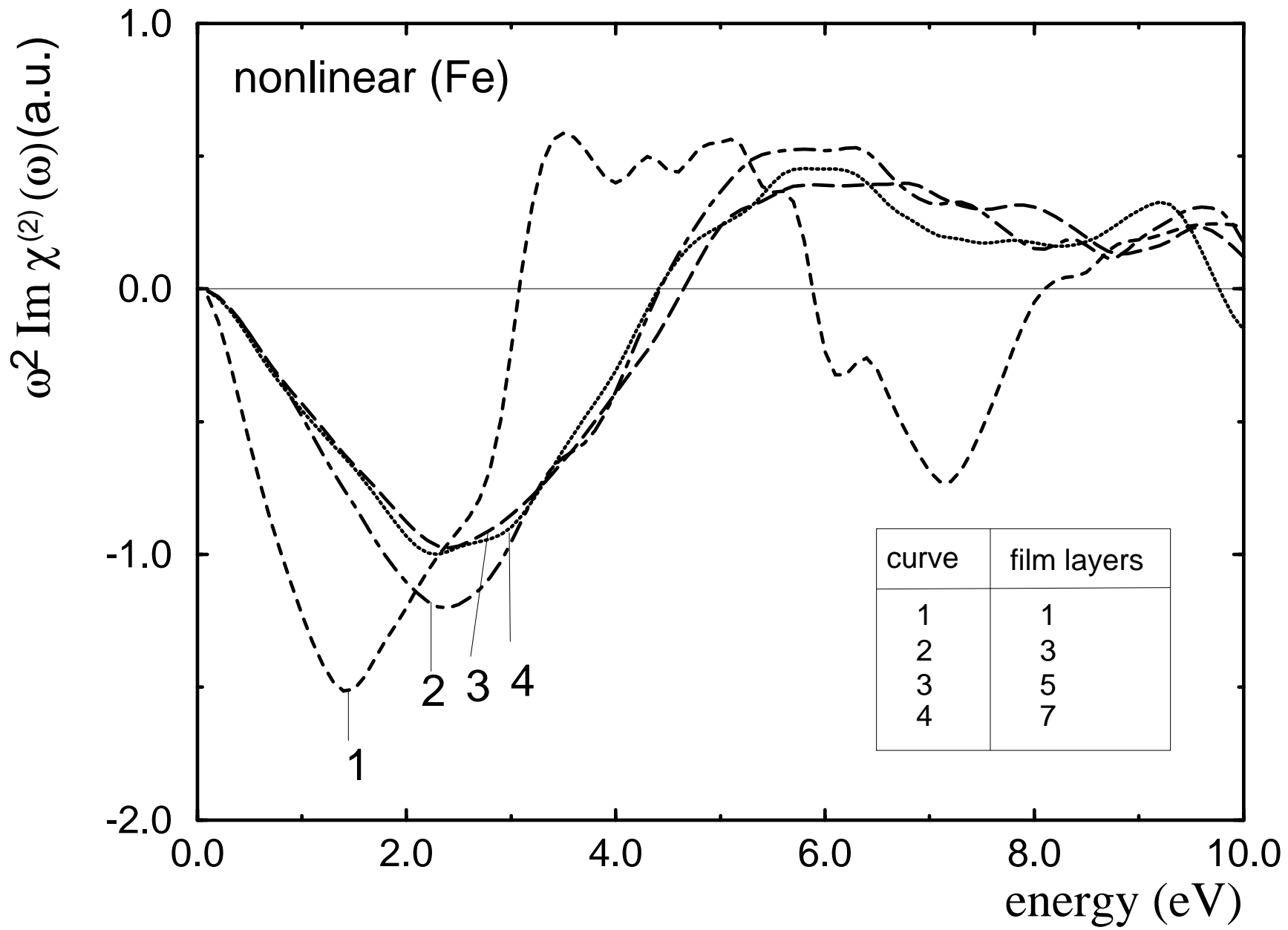


Fig. 1

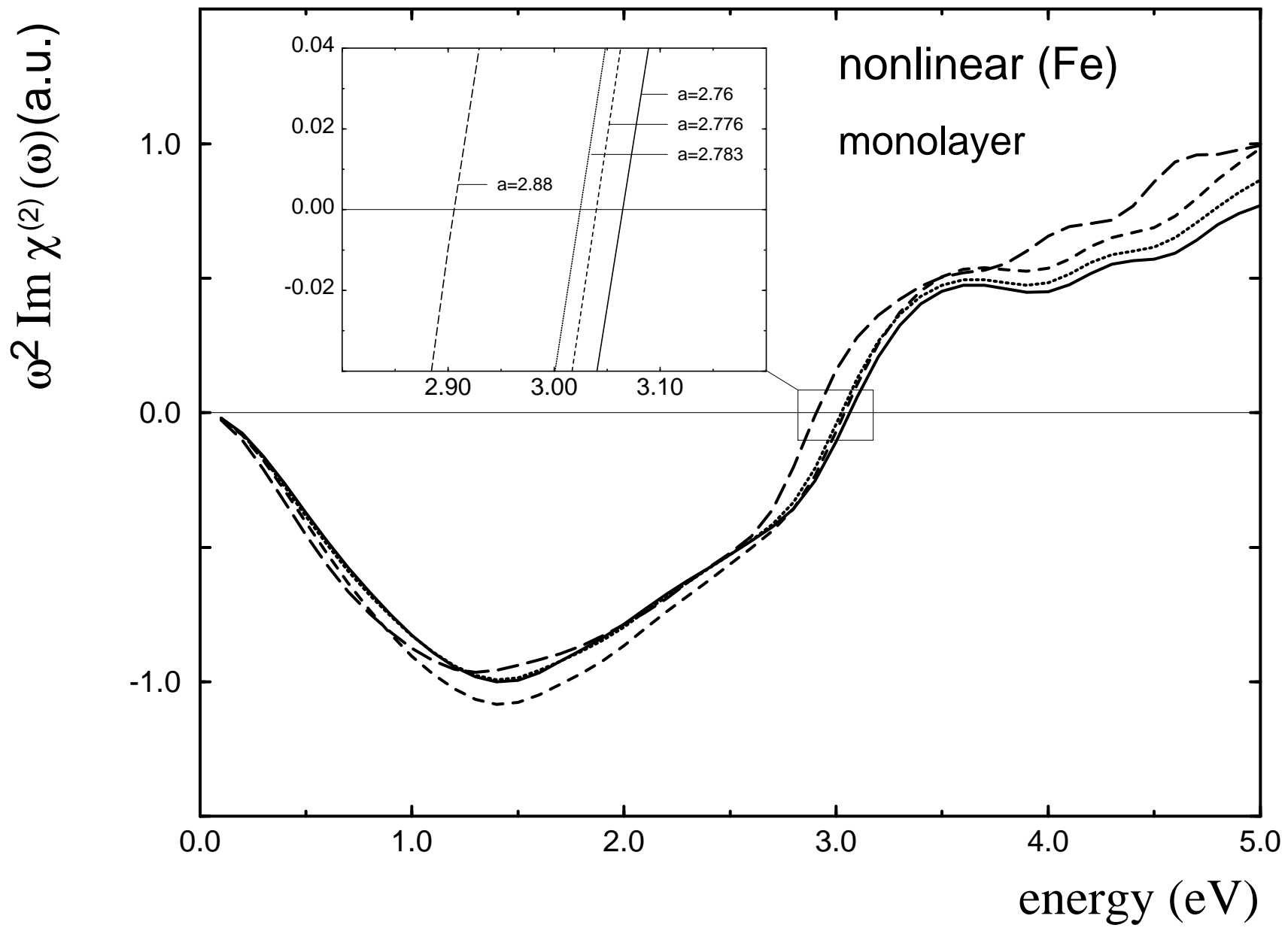
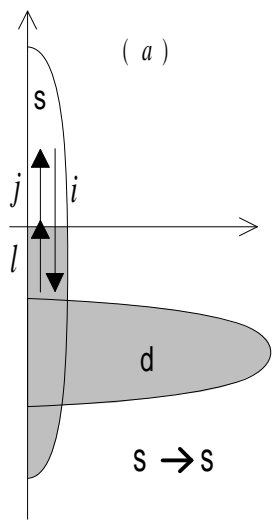
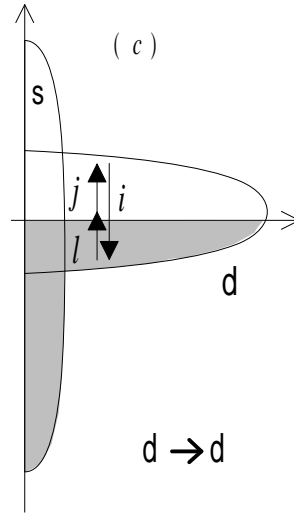
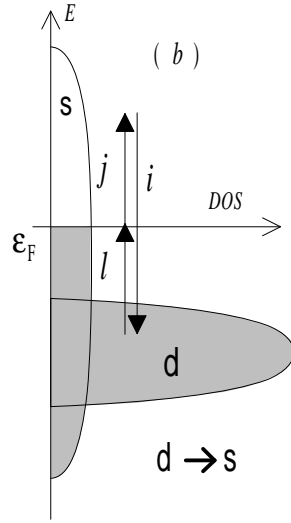


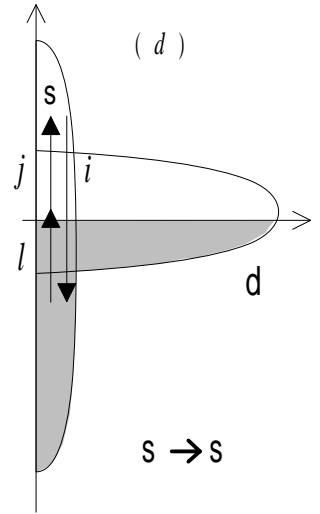
Fig. 2



Noble metals



Transition metals



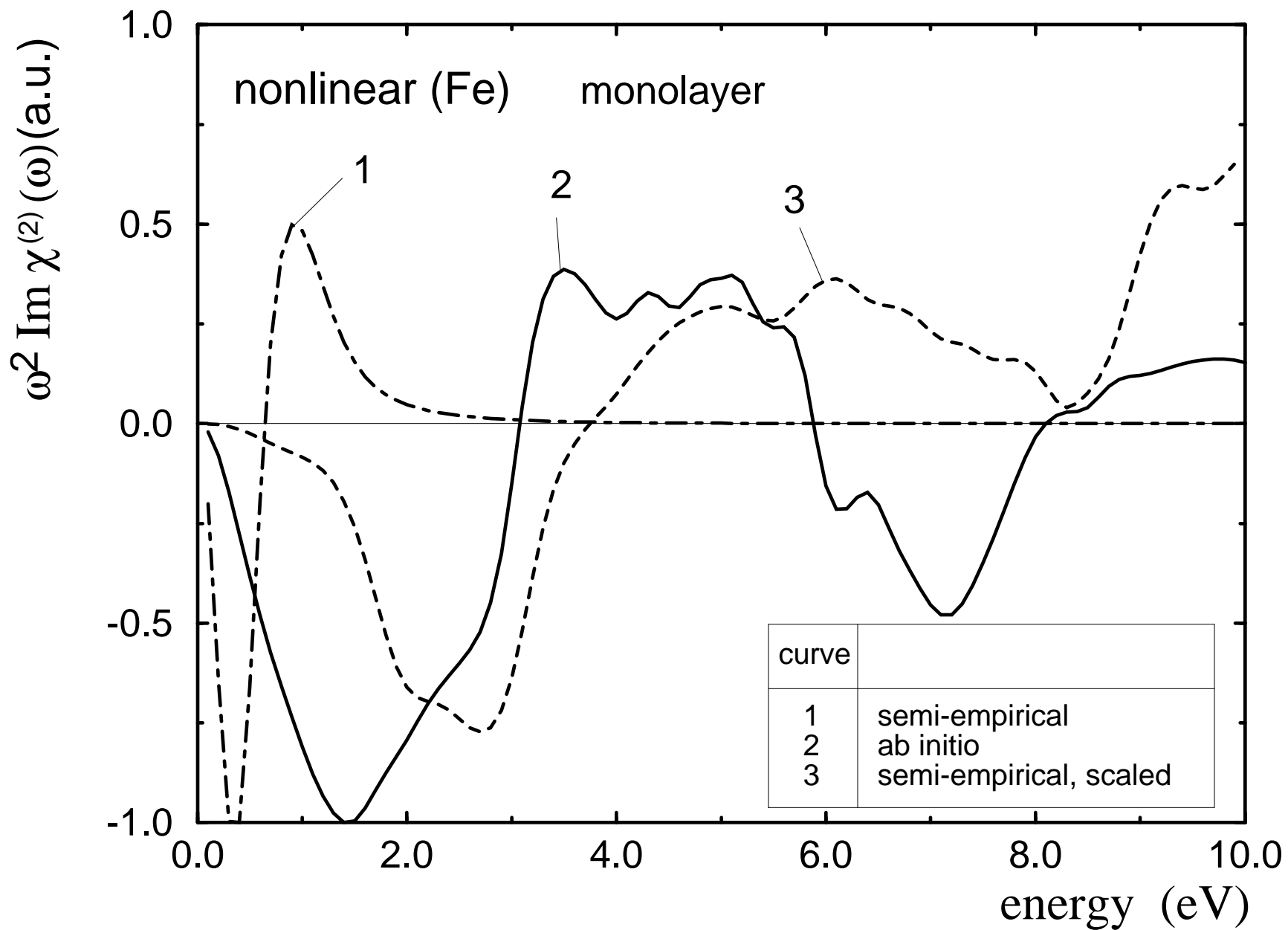
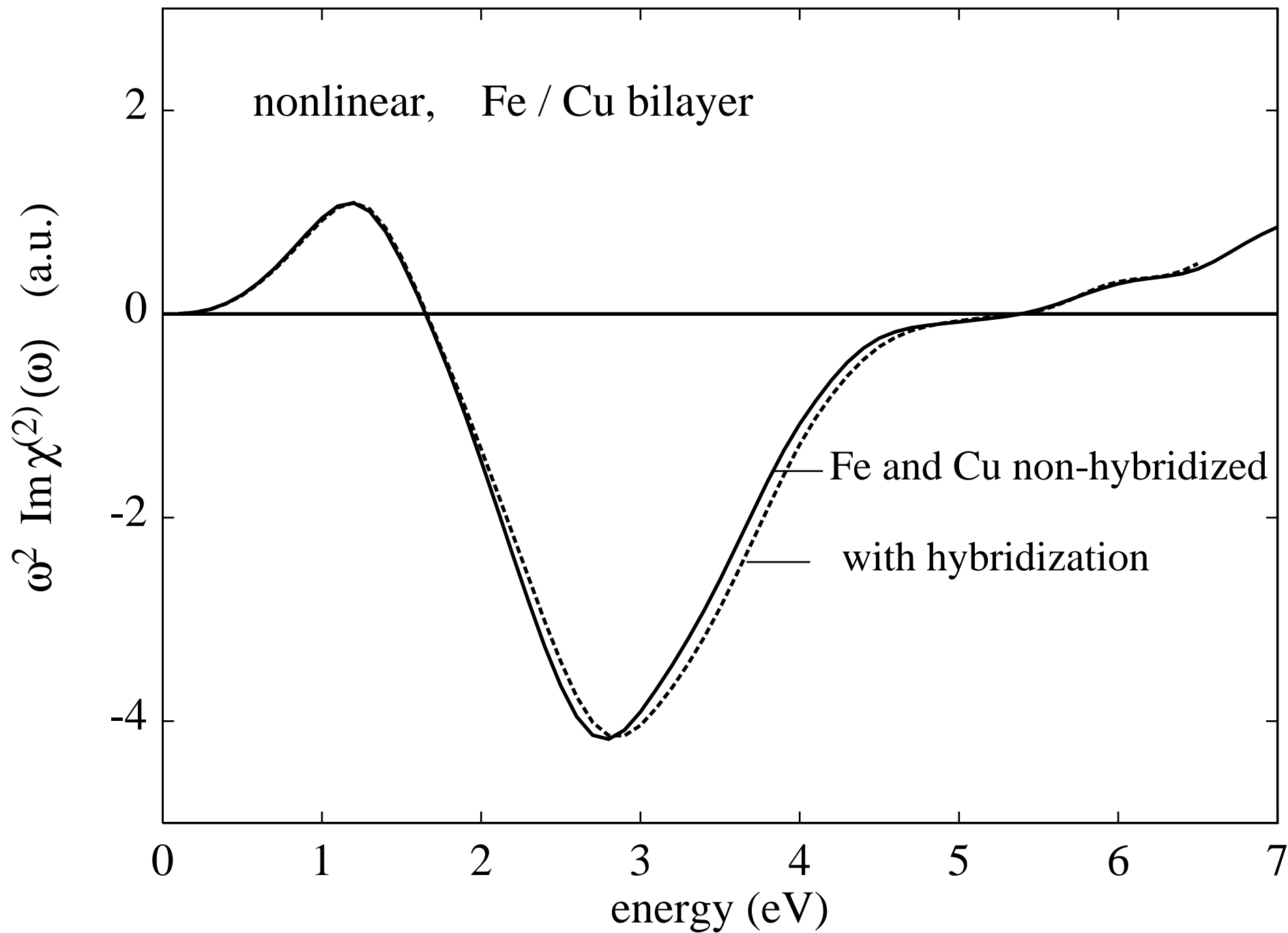


Fig. 3



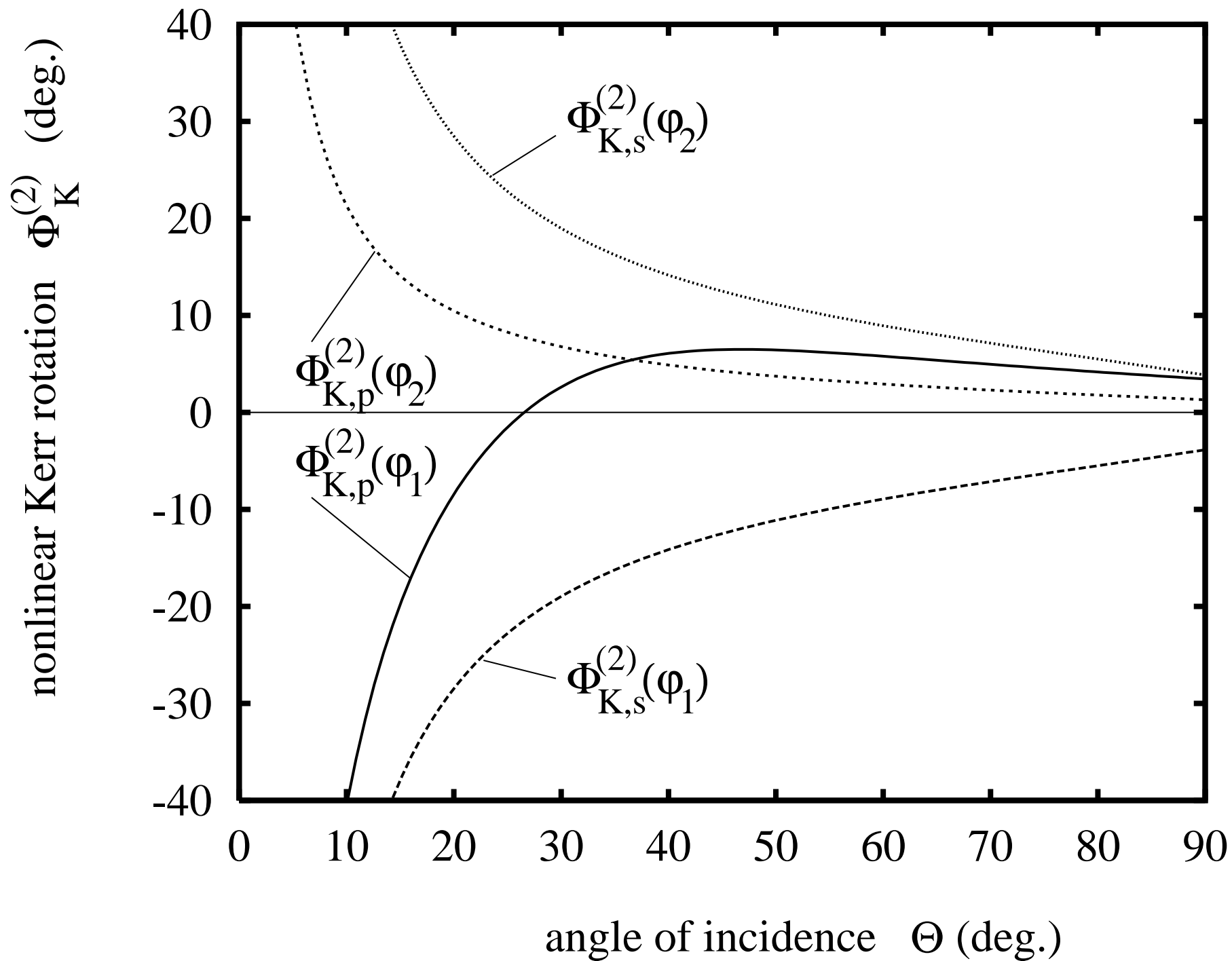


Fig. 6